J. Physiol. (1982), **322**, *pp.* 419–439
With 11 *text-figures*
Printed in Great Britain

PARACELLULAR NON-ELECTROLYTE PERMEATION DURING FLUID TRANSPORT ACROSS RABBIT GALL-BLADDER EPITHELIUM

BY MARTIN C. STEWARD*

From the Physiological Laboratory, Downing Street, Cambridge CB2 3EG

(*Received 1 April 1981*)

SUMMARY

1. Mucosa-to-serosa fluxes of seven polar non-electrolytes were determined during isotonic fluid transport across the unilateral rabbit gall-bladder preparation in an attempt to estimate the contribution of the paracellular pathway to the total transepithelial water flow.

2. ^{3}H- and ^{14}C-labelled non-electrolyte tracers appeared in the transported fluid at fractions (f_n) of their mucosal concentration which were inversely related to molecular size: ethanediol, 0·80; thiourea, 0·55; glycerol, 0·16; erythritol, 0·11; mannitol, 0·05; sucrose, 0·05; inulin, 0·02. The mean volume flow rate was 78 $\mu l \cdot cm^{-2} hr^{-1}$.

3. While the fluxes of the larger molecules were probably due to diffusion through a small but unrestricted paracellular 'shunt' permeability, the high f_n values obtained for the smaller molecules indicate the existence of a substantial paracellular permeability restricted to molecules smaller than erythritol.

4. Upper limits to the transcellular ethanediol and thiourea permeabilities, estimated from the time constants of tracer efflux from preloaded epithelial cells, were too low to account for more than a very small fraction of the transepithelial fluxes observed in the unilateral preparation.

5. Comparison of the f_n values with the predictions of a hydrodynamic model of paracellular permeation suggests that in order to account for the large fluxes of ethanediol and thiourea, considerably more than one half of the transepithelial water flow must follow the paracellular pathway.

6. Following a reduction of the mucosal osmolality to 110 m-osmole kg^{-1}, the apparent non-electrolyte permeability of the epithelium increased steadily over a period of 4 hr. This seems to reflect an increase in the shunt permeability rather than a change in the selectivity of the restricted permeability.

7. It is concluded that during isotonic fluid transport the bulk of the transepithelial water flow crossing the epithelium passes through paracellular channels of approximately 3 Å radius which are probably located in the intercellular junction.

* Present address: Department of Physiology, Stopford Building, University of Manchester, Manchester M13 9PT.

INTRODUCTION

The extent to which paracellular permeation routes across epithelia contribute to transepithelial water and solute transport has become a matter for speculation and investigation in a wide range of tight and leaky epithelia. In recent years, indications of solvent drag in the transepithelial permeation of extracellular markers such as sucrose have been noted in several epithelia responsible for isotonic fluid transport (Berry & Boulpaep, 1975; Hill & Hill, 1978*a*; Whittembury, Martinez, Linares & Paz-Aliaga, 1980; Hunter, Case, Steward & Young, 1981). These observations have generally been interpreted as indicating bulk water flow in the paracellular pathway, in contradiction to the assumptions underlying the standing-gradient osmotic flow hypothesis of Diamond & Bossert (1967). It has been pointed out however (Diamond, 1979), that whereas [^{14}C]sucrose appears in the fluid transported by the *Necturus* gall-bladder at very nearly the applied mucosal concentration (Hill & Hill, 1978*a*), the rabbit gall-bladder is relatively impermeable to sucrose except at very low osmolalities (Diamond, 1964*b*). The purpose of the present study, therefore, has been to investigate the permeation of the rabbit gall-bladder epithelium by a range of polar non-electrolyte molecules, during fluid transport, in an attempt to establish whether the difference between the two epithelia reflects a fundamental difference in mechanism, or simply a difference in the dimensions or 'selectivity' of the paracellular pathway.

In essence the approach is similar to that of Hill & Hill (1978*a*). Transported fluid (the absorbate) has been collected from the serosal surface of an isolated rabbit gall-bladder preparation bathed on its mucosal side by Ringer solution containing a tracer concentration of ^{14}C-labelled non-electrolyte. The ^{14}C activity of the absorbate has been determined as a fraction (the fractional transported concentration) of the mucosal activity, and results obtained for a range of polar non-electrolytes presumed to be restricted to the extracellular space. By comparing the fractional transported concentrations of the non-electrolytes with the predictions of a hydrodynamic model of paracellular permeation, it has proved possible to estimate both the effective radius or half-width of the channels through the intercellular junctions, and also the fraction of the total water flow that follows the paracellular route.

METHODS

Dissection. New Zealand White rabbits of either sex, weighing between 2·5 and 5 kg, were killed by cervical dislocation, and the gall-bladder and adjoining liver lobe removed to a dish of warm, oxygenated Ringer solution within a minute or two of death. In all of the experiments to be described, the gall-bladder was detached, emptied, cut open along the region previously attached to the liver, and washed several times to remove residual bile.

Solutions. Most of the experiments employed a bicarbonate/CO_2-buffered Ringer solution (Diamond, 1964*a*) of composition: NaCl, 110 mM; $NaHCO_3$, 25 mM; KCl, 7 mM; $CaCl_2$, 2 mM; $MgSO_4$, 1·2 mM; glucose, 11 mM; NaH_2PO_4, 1·2 mM. Oxygenation was provided and pH 7·4 maintained by gassing with a warmed, humidified mixture of 95% O_2 and 5% CO_2. Solutions of lower osmolality differed only in containing lower concentrations of NaCl. Osmolalities of 0·2 cm^3 samples were determined by freezing-point-depression osmometry (model 3 W, Advance Instruments) and are expressed in m-osmole kg^{-1} H_2O.

Radioactive tracers. [^{14}C]thiourea (60 mc m-mole^{-1}), [^{14}C]glycerol (51 mc m-mole^{-1}), [^{14}C]erythritol (101 mc m-mole^{-1}), [^{14}C]mannitol (58 mc m-mole^{-1}), inulin [^{14}C]carboxylic acid (8 mc m-mole^{-1}),

and [^{3}H]sucrose (5 c m-mole^{-1}) were obtained from the Radiochemical Centre, Amersham, and [^{14}C]ethanediol (4 mc m-mole^{-1}) from New England Nuclear (Dreieich, W. Germany). Inulin [^{14}C]carboxylic acid was passed through a gel-filtration column (Sephadex-G25, Pharmacia) before use in order to remove lower molecular weight contaminants, and [^{3}H]sucrose stock solutions were lyophilized at regular intervals to remove [^{3}H]water. Experimental samples were mixed with Biofluor scintillation fluid (New England Nuclear) and the ^{3}H and ^{14}C activities determined by liquid scintillation spectrometry (model 3255, Packard Instrument Co.).

Non-electrolyte fluxes in the unilateral preparation

The unilateral gall-bladder preparation, which allows direct sampling and analysis of the fluid transported by the epithelium, has traditionally consisted of a sac tied to the end of a cannula, and filled or perfused with Ringer solution (Diamond, 1964*b*; Hill & Hill, 1978*a*, *b*; Whittembury *et al.* 1980). In the investigation described here, an alternative arrangement was employed in order to improve stirring, temperature control and oxygenation, and to minimize transmural pressure differences. The preparation consisted of a flat sheet of gall-bladder wall, of area 1·43 cm^2, held stretched over the mouth of a small, rimmed glass funnel with the mucosal surface of the tissue facing outwards (Fig. 1). A concentric double polythene sampling cannula connected to the stem of the funnel allowed the withdrawal of absorbate samples, usually at hourly intervals, while the whole chamber remained submerged in a reservoir of Ringer solution. The latter, normally 20 cm^3 in volume, was stirred by a stream of warmed humidified gas bubbles, and a temperature of 37 °C maintained by a thermostatically controlled dry-block incubator (model DB-3, Techne Ltd).

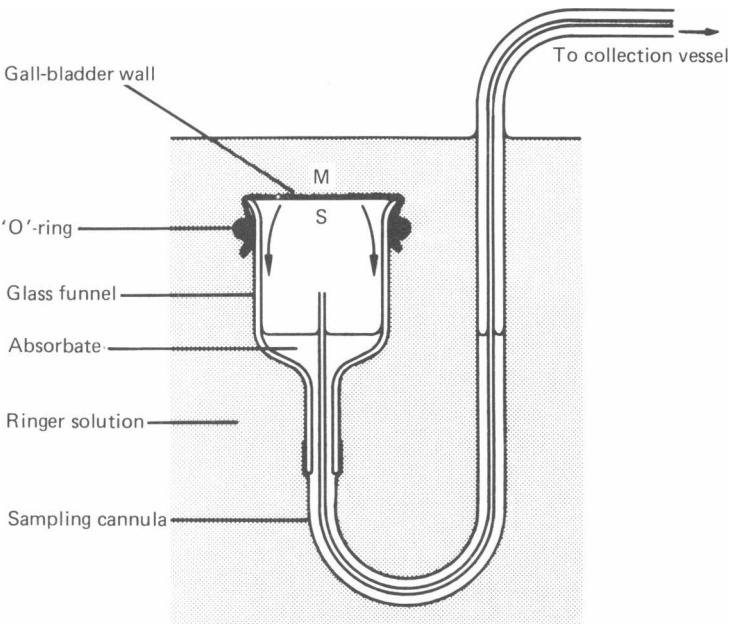

Fig. 1. Mounting arrangement for the unilateral gall-bladder preparation. Absorbate drains from the serosal surface (S) into the stem of the glass funnel and may be withdrawn through the outer section of the sampling cannula into a closed vessel (not shown). The fine central cannula provides continuity between the atmosphere and the funnel interior. The funnel diameter is 1·3 cm, and the epithelium is generally positioned less than 1 cm from the surface of the Ringer solution. (M: mucosal surface.)

In order to determine mucosa-to-serosa fluxes during fluid transport, tracer concentrations of ^{14}C- and ^{3}H-labelled non-electrolytes (usually less than 10 μM) were added to the mucosal Ringer solution shortly after mounting the preparation. One hour after the addition of the tracers, the absorbate which had accumulated in the stem of the funnel, and which would be expected to contain the bulk of the tracer-free fluid previously occupying the serosal dead space, was withdrawn and

discarded. By this time the non-electrolyte fluxes were assumed to have reached their approximately steady-state levels and the absorbate that accumulated over the course of the following hour was withdrawn and weighed in order to estimate the mean volume flow rate J_v. 75 μl. samples of the absorbate and the mucosal fluid were then each mixed with 3 cm^3 of scintillation fluid and assayed for ^{14}C and ^3H activity. In experiments designed to monitor changes in the non-electrolyte fluxes following a reduction in mucosal fluid osmolality, identical concentrations of the non-electrolyte tracers were included in the normal- and low-osmolality Ringer solutions and hourly absorbate samples collected for a total of five hours.

Non-electrolyte fluxes expressed as fractional transported concentrations f_n have been calculated from the measured absorbate and mucosal tracer activities according to

$$f_n = \frac{\text{Absorbate activity (cpm cm}^{-3})}{\text{Mucosal activity (cpm cm}^{-3})} \quad (1)$$

and results are presented as the means (±S.E. of mean) of data from at least four different gall-bladders.

Non-electrolyte efflux measurements

Gall-bladders removed, emptied and rinsed as above were divided into two pieces and rinsed for a further 15 min in oxygenated Ringer solution. Each piece was then incubated for 1 or 2 hr in 2 cm^3 Ringer solution containing 5 μc ^{14}C-labelled urea, ethanediol or thiourea. 100 μl. samples of the incubation solutions were retained as standards for subsequent scintillation assay. A temperature of 37 °C was maintained throughout and agitation was provided by vigorous gassing. Following the loading period and a preliminary 5 min rinse in 20 cm^3 of label-free Ringer solution, tissue pieces were taken through a series of 5 or 10 min rinses in 1·5 cm^3 Ringer solution. 1 cm^3 samples taken from each of the rinsing solutions were mixed with 8 cm^3 of scintillation fluid and assayed for ^{14}C activity together with the appropriate blanks and standards. Finally, the tissue pieces were swabbed with damp filter paper and their wet weights determined with 0·1 mg accuracy.

After correction for background activity, mean non-electrolyte efflux rates were calculated for each rinse period and plotted on a log scale as a function of time. The time constant and integral of the slow component of efflux were estimated by least-squares linear regression on the assumption that the slow component follows an exponential time course:

$$J_e = J_{e,0} \exp(-t/\tau_{slow}), \quad (2)$$

where $J_{e,0}$ is the efflux rate immediately following the loading period ($t = 0$). The apparent volume of the compartment responsible for the slow component was calculated from the integral and corrected for the loading period on the assumption that during the loading period, the tracer concentration C_i inside the compartment approached the external, loading concentration C_o according to an exponential time course with the same time constant as that observed during efflux:

$$C_i = C_o(1-\exp(-t/\tau_{slow})). \quad (3)$$

For reasons to be discussed below, no attempt was made to correct for the effects of unstirred layers.

Simulation of paracellular non-electrolyte flow

Programmes written in Fortran IV were run in double precision on the IBM 370/165 computer of the University of Cambridge Computing Service, using routine D02CAF of the Numerical Algorithms Group Library to integrate the differential equation for interspace non-electrolyte flow (eqns. (A 15) and (A 16)).

In calculating the expected paracellular fluxes of the various non-electrolytes it was assumed: (1) that their free-solution diffusion coefficients D_n are related to molecular weight M by the relationship $D_n M^{0.5}$ = a constant (Stein, 1967) with $D_n = 5{\cdot}2 \times 10^{-6}$ cm^2 sec^{-1} for sucrose as a reference (Longsworth, 1953); and (2) that their hydrodynamic radii a may be estimated from their diffusion coefficients by means of the Stokes-Einstein relationship and the small-molecule correction of Schultz & Solomon (1961)

$$a = \frac{a_{SE} + \sqrt{(a_{SE}^2 + 2a_{SE})}}{2}, \quad (4)$$

where a_{SE} is the Stokes-Einstein radius of the molecule. Values of M, D_n and a for each of the non-electrolyte tracers are listed in Table 1.

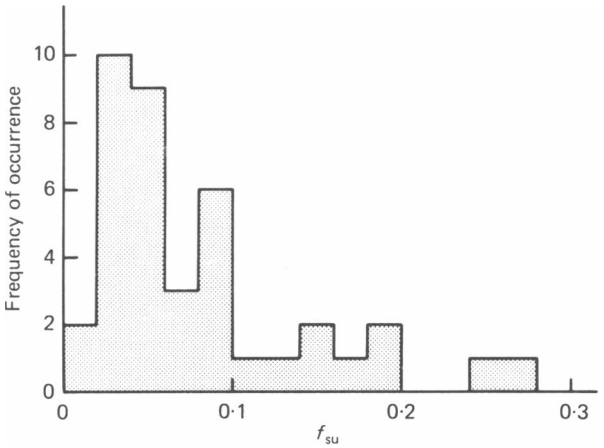

Fig. 2. Distribution of the values of the fractional transported concentration of [^{3}H]sucrose obtained in thirty-nine experiments. The absorbate samples were each collected over a period of 1 hr.

TABLE 1. Molecular properties, fractional transported concentrations (f_n) and apparent permeability coefficients (P_n') of the tracer non-electrolytes

	M	$10^6 D_n$ (cm^2 sec^{-1})	a (Å)	f_n	f_{su}	J_v ($\mu l\ cm^{-2}$ hr^{-1})	$10^6 P_n'$ (cm sec^{-1})	n
Ethanediol	66	11·8	2·5	0·796±0·015	0·078±0·008	82±11	93·3±14·9	5
Thiourea	78	10·9	2·6	0·550±0·043	0·048±0·011	70±7	26·7±6·7	5
Glycerol	94	9·9	2·9	0·157±0·029	0·040±0·008	94±9	5·48±1·60	5
Erythritol	125	8·6	3·2	0·108±0·012	0·051±0·011	60±9	1·94±0·22	5
Mannitol	184	7·1	3·9	0·052±0·007	0·039±0·006	76±11	1·12±0·14	5
Sucrose	342	5·2	5·1		0·050±0·004	78±5	1·10±0·11	30
Inulin	5200	*1·3		0·017±0·004	0·044±0·009	86±13	0·34±0·04	5

The molecular weights (M) are those of the radiolabelled molecules, and the free-solution diffusion coefficients (D_n) and hydrodynamic radii (a) were obtained as described in the methods section.
* From Phelps (1965).

RESULTS

Non-electrolyte permeation during fluid transport at normal osmolality

Fractional transported concentrations (f_n) of [^{3}H]sucrose and ^{14}C-labelled ethanediol, thiourea, glycerol, erythritol, mannitol and inulin were determined in a series of thirty-nine experiments using the unilateral rabbit gall-bladder preparation. In each experiment values of f_n were obtained simultaneously for both [^{3}H]sucrose and one of the ^{14}C-labelled non-electrolytes. The [^{3}H]sucrose value f_{su} was measured both as a reference for subsequent analysis, and also as a convenient means of assessing the structural integrity of the preparation. Fig. 2 illustrates the distribution of the f_{su} values drawn from all thirty-nine experiments, and it is evident that whilst 30 (77 %) of the preparations yielded values in the range 0−0·1, consistent with the previous observation that 'the secreted fluid contained only small or barely detectable quantities of sucrose' (Diamond, 1964*b*), several yielded rather higher values. In some cases this was due to unusually low volume flow rates; in others it may have reflected

real differences between the epithelia of different individuals. It is, however, also possible that it was occasionally a consequence of edge-damage or damage sustained during mounting. For this reason, and in order to permit the comparison of mean f_n values based on relatively small sample groups, the nine experiments in which f_{su} exceeded 0·1 were excluded from further analysis.

The mean fractional transported concentrations (f_n) of the ^{14}C-labelled non-electrolytes are listed in Table 1, together with the accompanying mean f_{su} values and mean volume flow rates (J_v) obtained in each group of five experiments. It may be noted that the group means for f_{su} and J_v are scattered slightly around the over-all mean values drawn from all thirty experiments.

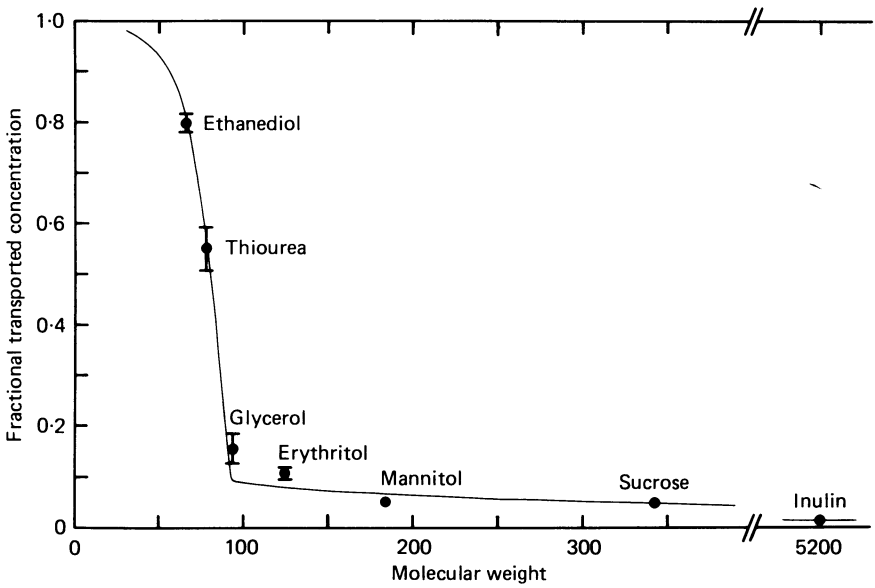

Fig. 3. Mean fractional transported concentrations (±S.E. of mean) of seven polar non-electrolytes plotted as a function of molecular weight. $n = 5$ for each non-electrolyte except sucrose for which $n = 30$. Error bars smaller than the symbol radii are omitted. The curve was generated by a hydrodynamic model of non-electrolyte flow in the paracellular pathway (see legend to Fig. 7*A*).

The dependence of f_n on molecular weight is illustrated in Fig. 3. Three features are particularly evident: (1) the high f_n values for ethanediol and thiourea; (2) the steep 'cut-off' at molecular weights of around 80; and (3) the long 'tail' of low permeability to the larger non-electrolytes.

It is quite clear that a non-electrolyte selectivity pattern of this sort cannot be accounted for simply in terms of an unrestricted, diffusive shunt or leak pathway across the epithelium. In the steady state the flux of a non-electrolyte J_n through such a pathway would depend on the mucosal and serosal concentrations $C_n(M)$ and $C_n(S)$, and the non-electrolyte permeability coefficient P_n, according to

$$J_n = P_n(C_n(M) - C_n(S)) \tag{5}$$

and the permeability coefficients of the different non-electrolytes, all else being equal, would be directly related to their free-solution diffusion coefficients D_n. Now since

$J_n = C_n(S) J_v$ and $C_n(S) = f_n C_n(M)$, apparent permeability coefficients P_n' for the various non-electrolytes tested may be calculated from the experimental data using

$$P_n' = J_v f_n/(1-f_n) \tag{6}$$

and in each individual experiment, therefore, where J_v is constant

$$\frac{P_n'}{P_{su}'} = \frac{f_n/(1-f_n)}{f_{su}/(1-f_{su})}. \tag{7}$$

Mean values of this ratio for each of the ^{14}C-labelled non-electrolytes have been plotted against D_n/D_{su} in Fig. 4 to test the hypothesis that permeation occurs via an unrestricted diffusive permeability. P_n'/P_{su}' approximates closely to D_n/D_{su} for

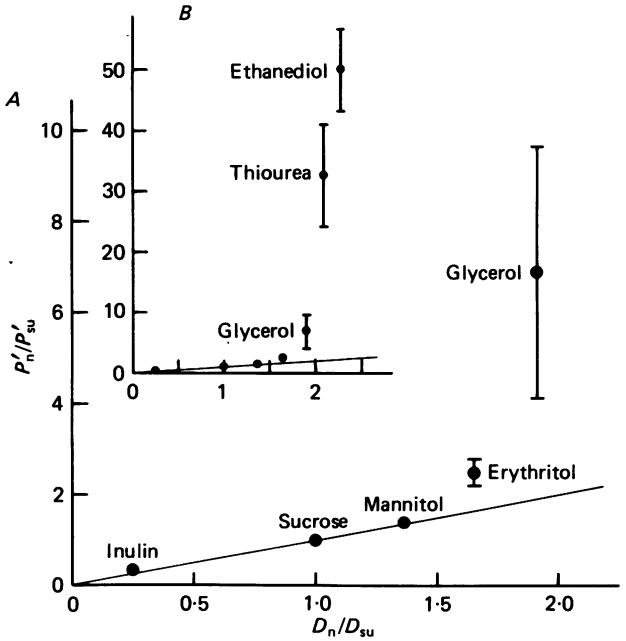

Fig. 4. *A*, relationship between the apparent non-electrolyte permeability ratio P_n'/P_{su}' and the free-solution diffusion coefficient ratio D_n/D_{su}. *B*, the same, but including the data points for thiourea and ethanediol which lie some distance from the line of identity. Each point represents the mean (±S.E. of mean) of five measurements.

inulin, sucrose and mannitol, and these molecules may therefore, as has been suggested before (Smulders & Wright, 1971; van Os, de Jong & Slegers, 1974), permeate by diffusion through such a pathway (hereafter referred to as the 'shunt' pathway). The smaller non-electrolytes, however, cross the epithelium at rates vastly in excess of what would be expected of the shunt pathway alone. This could be due to the existence of an additional but restricted paracellular permeability, or alternatively it could indicate transcellular non-electrolyte permeation.

Cellular non-electrolyte efflux measurements

According to the osmotic reflexion coefficient measurements of Wright & Diamond (1969), ethanediol and thiourea are neither small enough nor lipid soluble enough to

penetrate the cell membranes of the rabbit gall-bladder epithelium very readily. It would therefore seem unlikely that a transcellular permeation pathway could acount for the very high apparent permeabilities to these molecules observed in the fluid-transporting unilateral preparation. Nonetheless, in order to assess this possibility quantitatively, the time constants of cellular efflux of ^{14}C-labelled urea, ethanediol and thiourea have been determined in a series of experiments in which pieces of gall-bladder wall were loaded with the tracers for 1 or 2 hr prior to the efflux measurement.

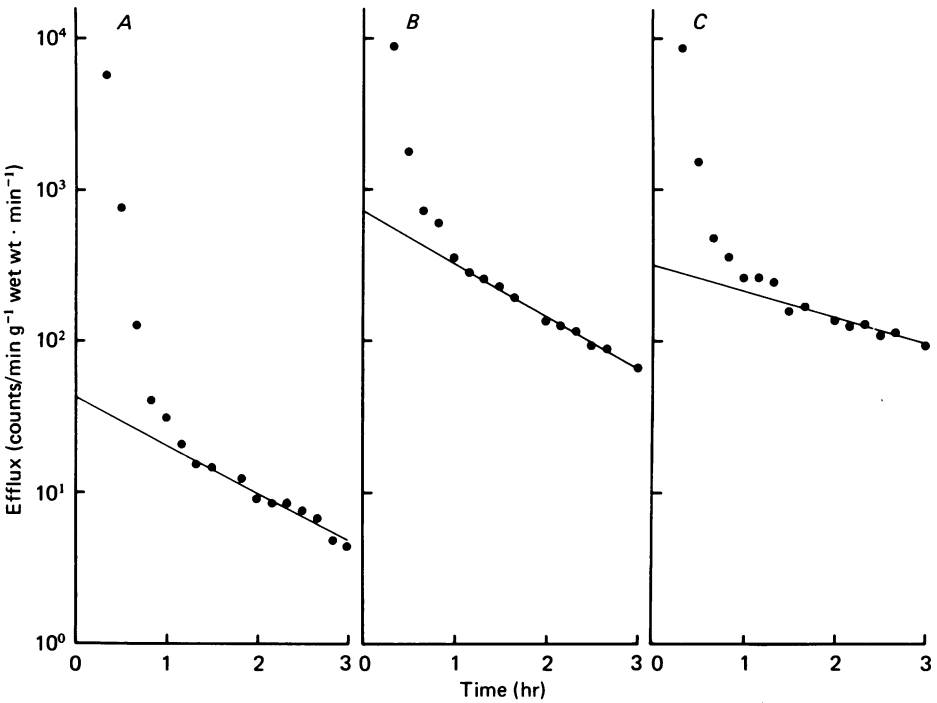

Fig. 5. Efflux of ^{14}C-labelled non-electrolytes from hemibladders preloaded with the tracers for 1 hr. The slow exponential components of efflux were fitted by least-squares linear regression. *A*, urea: $\tau_{slow} = 83$ min, $V_{slow} = 2\ \mu l.g^{-1}$, $r = 0{\cdot}978$, $P < 0{\cdot}001$. *B*, thiourea: $\tau_{slow} = 75$ min, $V_{slow} = 46\ \mu l.g^{-1}$, $r = 0{\cdot}996$, $P < 0{\cdot}001$. *C*, ethanediol: $\tau_{slow} = 149$ min, $V_{slow} = 59\ \mu l.g^{-1}$, $r = 0{\cdot}967$, $P < 0{\cdot}001$.

Fig. 5 illustrates typical time courses of tracer efflux from three preloaded hemibladder pieces which were taken through a series of 10 min washes in ^{14}C-free Ringer solution. In each case the fast exponential component of efflux, accounting for the majority of the tracer recovered, almost certainly derived from the extracellular compartment. The slower exponential component seen clearly in the efflux of ethanediol and thiourea, however, probably reflects non-electrolyte efflux from an intracellular compartment. The time constants of the slow component τ_{slow} and the corresponding apparent compartment volumes V_{slow} (corrected for the limited loading period and expressed in $\mu l.g^{-1}$ wet weight) have been determined by least-squares linear regression, and the mean values obtained for urea, ethanediol and thiourea are listed in Table 2.

The calculated compartment volume for ethanediol and thiourea corresponds well with that expected from the stereological measurements of Blom & Helander (1977). Also, the ratio of the mean time constants for ethanediol and thiourea efflux is comparable with the inverse ratio of their olive oil:water partition coefficients, suggesting that these non-electrolytes have to cross a lipid barrier in order to leave the tissue. The results obtained with urea do not fit this interpretation, possibly because a fast efflux from the cells becomes confounded with the movement of urea from the extracellular space.

TABLE 2. Time constants (τ_{slow}) and calculated compartment volumes (V_{slow}) of the slow component of non-electrolyte tracer efflux

	M	K_{oil}	τ_{slow} (min)	V_{slow} (μl g^{-1} wet wt.)	n
Urea	62	0·00015	63±5	5±1	5
Ethanediol	66	0·00049	132±12	36±5	6
Thiourea	78	0·0012	76±7	42±3	7

Olive oil:water partition coefficients (K_{oil}) from Collander (Wright & Diamond, 1969).

In order to estimate the transcellular permeabilities to ethanediol and thiourea from the efflux data it will be assumed that tracer efflux from the intracellular compartment of 1 cm^2 of epithelium is satisfactorily described by

$$J_e = V\,dC_i/dt = P_e C_i \tag{8}$$

where V is the volume of the intracellular compartment per cm^2, P_e the efflux permeability per cm^2, and C_i the intracellular tracer concentration. The efflux J_e is thus described as a function of time by

$$J_e = J_{e,0} \exp(-t/\tau_e) \tag{9}$$

in which $J_{e,0}$ is the efflux at $t = 0$, and τ_e the time constant of efflux

$$\tau_e = V/P_e. \tag{10}$$

Now the transcellular permeability to a non-electrolyte P_t depends to a first approximation on the reciprocal sum of the apical and basolateral membrane permeabilities P_a and P_b:

$$1/P_t = 1/P_a + 1/P_b \tag{11}$$

while the efflux permeability P_e depends on the direct sum

$$P_e = P_a + P_b. \tag{12}$$

Thus if the apical and basolateral membranes contribute fractions α and $1-\alpha$ to the total efflux permeability, then from eqns. (10), (11) and (12):

$$P_t = \alpha(1-\alpha)\,V/\tau_e. \tag{13}$$

As the relative non-electrolyte permeabilities of the apical and basolateral membranes are not known, it is difficult to estimate α, but since by definition $\alpha(1-\alpha)$ cannot exceed 0·25, it is nonetheless possible to determine an upper limit to the magnitude of the transcellular permeability:

$$P_t < 0{\cdot}25\,V/\tau_e. \tag{14}$$

This derivation ignores the effects of unstirred layers on the grounds that the unstirred layers hindering cellular efflux and those hindering transcellular permeation are effectively identical and therefore may be considered simply as integral components of the apical and basolateral permeabilities P_a and P_b.

Now if the volume of the cellular compartment may be taken as 2 μl . cm^{-2}, eqn. (14) suggests that, given the measured efflux time constants, the transcellular permeabilities to ethanediol and thiourea cannot exceed approximately $6{\cdot}3 \times 10^{-8}$ cm sec^{-1} and $1{\cdot}1 \times 10^{-7}$ cm sec^{-1} respectively. As both figures are two or three orders of magnitude smaller than the apparent permeabilities seen in the unilateral preparation during fluid transport (Table 1), it would seem unlikely that transcellular permeation accounts for more than a very small fraction of the ethanediol and thiourea fluxes observed under those conditions.

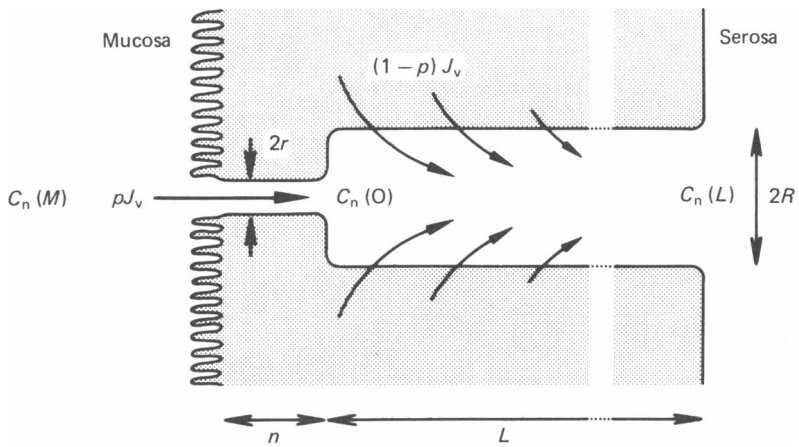

Fig. 6. Schematized longitudinal section of the paracellular pathway. In the model employed in this study, the paracellular water flow pJ_v enters the interspace through the junctional complex, and the transcellular water flow $(1-p)J_v$ enters through the lateral cell membranes according to a standing-gradient flow pattern.

Simulation of paracellular non-electrolyte permeation

In order to test the alternative hypothesis, that the very high apparent permeabilities to ethanediol and thiourea are due to the existence of narrow channels through the intercellular junctions (in parallel with the unrestricted shunt permeability), a simulation of non-electrolyte flow in the paracellular pathway has been used to interpret the selectivity pattern of Fig. 3. The restricted junctional channels of 1 cm^2 of epithelium have been considered both as an array of N pores of radius r and depth n, and also as a network of parallel-sided slits of half-width r, depth n and linear extent s in the plane of the epithelium. This treatment of the paracellular pathway, of which a schematic section is shown in Fig. 6, is described fully in the Appendix. In order to interpret the non-electrolyte selectivity pattern of Fig. 3, values of f_n have been calculated as a function of molecular weight over the range 70–350. Selectivity curves have been computed for both slit and pore models using a wide range of values for the junctional parameters r, s/n (slit) and N/n (pore), and values of 0, 0·5, and 1 for the fraction p of the total water flow J_v, passing through the junctional channels. J_v has been taken as 78 μl . cm^{-2} hr^{-1} (Table 1).

Comparison of the experimental data with selectivity curves such as those illustrated in Fig. 7 leads to three general conclusions. (1) The very steep fall in f_n at molecular weights of around 80 suggests that the restricted channels, whether they be slits or pores, have an effective half-width or radius of approximately 3 Å. (2) The high values of f_n characteristic of ethanediol and thiourea can only be explained if the fraction of the total water flow that passes through the junctional channels is substantially greater than 0·5. (3) The values of s/n and N/n required by the slit and pore models respectively for such a steep dependence of f_n on molecular weight are

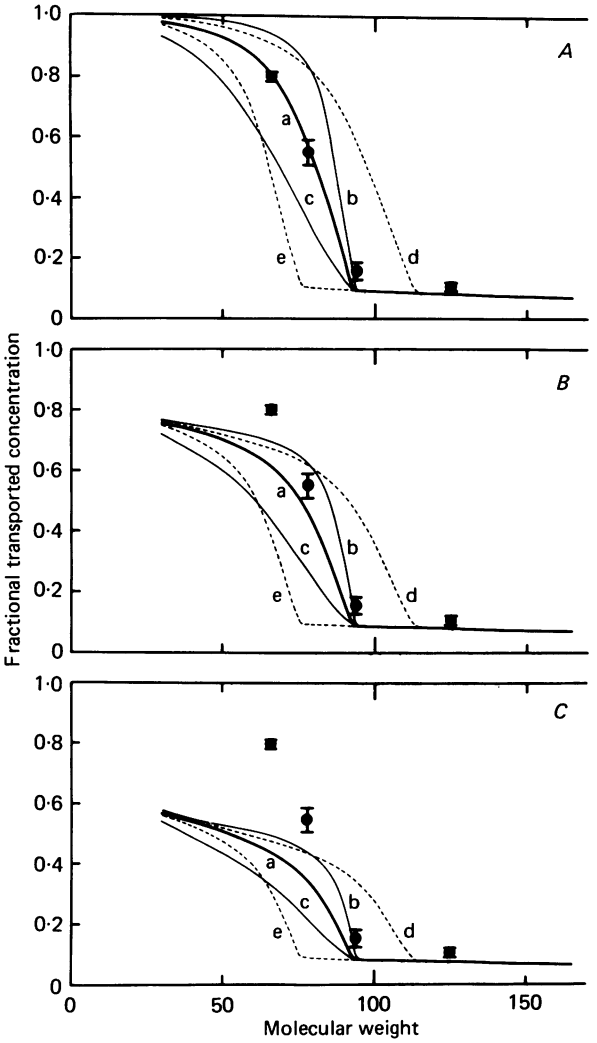

Fig. 7. Comparison of non-electrolyte selectivity patterns predicted by the junctional slit model with experimental data for ethanediol, thiourea, glycerol, and erythritol (see Fig. 3). *A*, exclusively paracellular water flow ($p = 1$). Curve a: $r = 2{\cdot}85$ Å, $s/n = 3{\cdot}6 \times 10^9$ cm^{-2}. Curves b and c illustrate the effects of increasing and decreasing the value of s/n by a factor of 4. Curves d and e illustrate the effects of increasing and decreasing the channel half-width r by 0·25 Å. *B*, mixed paracellular and transcellular water flow ($p = 0{\cdot}5$). Curves as in *A*. *C*, exclusively transcellular water flow ($p = 0$). Curves as in *A*. In every case, $J_v = 78\ \mu$l. cm^{-2} hr^{-1}, and the shunt component is based on $P_{su}' = 1{\cdot}14 \times 10^{-6}$ cm sec^{-1}.

of the order of $3{\cdot}6 \times 10^9$ cm^{-2} and $3{\cdot}3 \times 10^{18}$ cm^{-3}. This means that if the maximum geometrically reasonable values of s and N are taken as 4000 cm cm^{-2} and $4000/2r$ cm^{-2}, the maximum channel depth n compatible with the experimental data will be 110 Å for the slit model and 2 Å for the pore model. The latter seems implausibly small so it may perhaps be concluded tentatively that the restricted channels show a selectivity more like that expected of a slit network than a population of cylindrical pores.

Non-electrolyte permeation during fluid transport at reduced osmolality

It has been demonstrated by Diamond (1964*b*) that the unilateral rabbit gall-bladder preparation continues to transport an almost isotonic fluid when the osmolality of the mucosal Ringer solution, normally about 290 m-osmole kg^{-1}, is reduced to as little

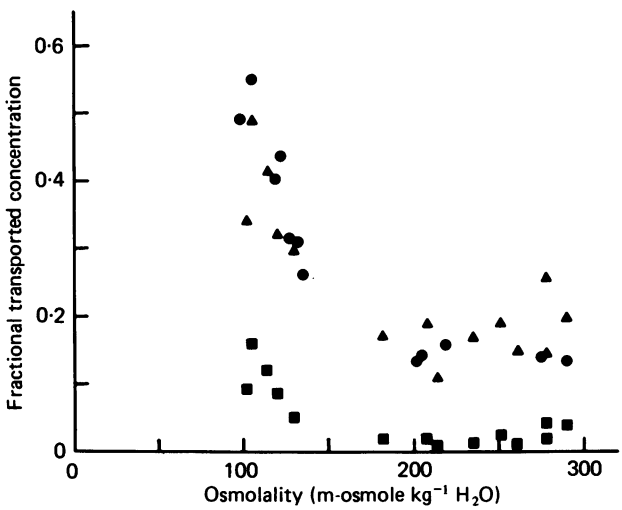

Fig. 8. Osmolality dependence of the fractional transported concentrations of sucrose (●), fucose (▲), and inulin (■) tracers. Collection periods ranged between 3 and 6 hr.

as 80 m-osmole kg^{-1}. He has also pointed out, however, that at low osmolalities the epithelium becomes 'leaky' to phenol red and sucrose (Diamond, 1964*b*, 1979). In an attempt to understand this latter phenomenon in terms of the model for non-electrolyte permeation described in this paper, the fractional transported concentrations of several non-electrolytes have been measured first as a function of mucosal osmolality and second as a function of time during transport at reduced osmolality.

Using data from a preliminary study, fractional transported concentrations of inulin, sucrose and fucose, based on single absorbate samples collected over periods of 3–6 hr, are plotted against mucosal osmolality in Fig. 8. A quite distinct rise in f_n for each non-electrolyte is evident at osmolalities below about 150 m-osmole kg^{-1}, although this is partly attributable to the rather low mean volume flow rates observed over periods of 3–6 hr at these osmolalities. Below about 90 m-osmole kg^{-1} fluid transport was generally not sustained long enough for collection of a sufficient volume of absorbate.

Fig. 9*A* illustrates the results of twenty-four experiments in which, after 1 hr at normal osmolality, the mucosal osmolality was reduced to 110 m-osmole kg^{-1} by removal of NaCl, and samples of absorbate collected every subsequent hour for a total of 4 hr. In Fig. 9*B* the gradual rise in the apparent permeability to sucrose over that period is compared with the fairly constant permeability seen in the averaged results of four control experiments. The combined effects of the increase in shunt permeability and the concurrent changes in J_v (Fig. 9*C*) on the non-electrolyte selectivity pattern predicted by the slit model are compared in Fig. 10 with the experimental data from the first, third and fifth hours of the time-course experiments. It would seem that a gradually increasing shunt permeability is well able to account for the change in the fractional transported concentration of each of the non-electrolytes examined.

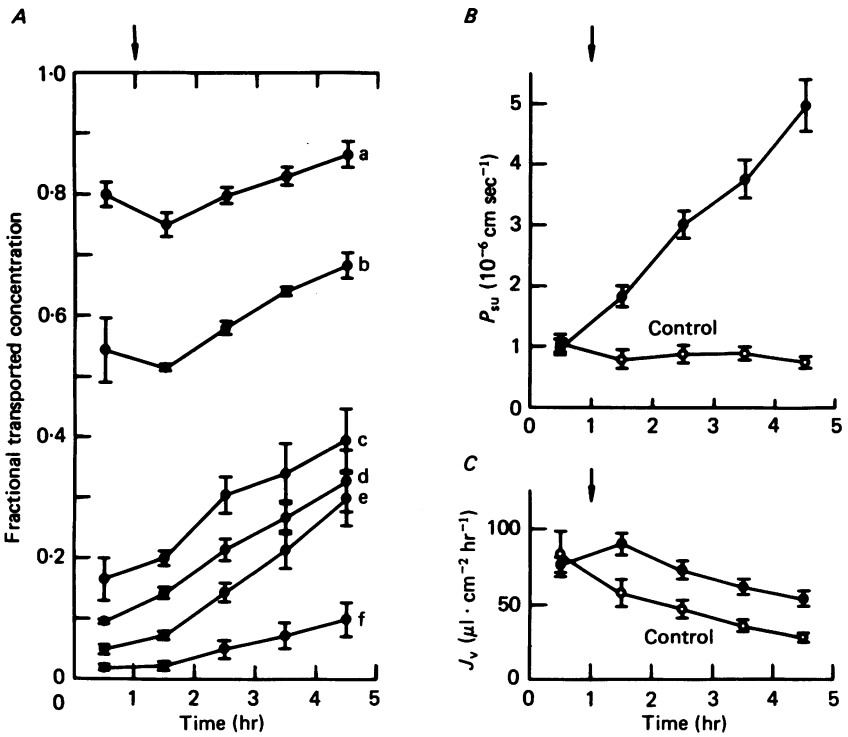

Fig. 9. Effects of reducing the mucosal osmolality from normal (290 m-osmole kg^{-1}) to 110 m-osmole kg^{-1} after 1 hr as indicated by the arrows. *A*, mean fractional transported concentrations (±S.E. of mean, $n = 4$) of: (*a*) ethanediol; (*b*) thiourea; (*c*) glycerol; (*d*) erythritol; (*e*) mannitol; (*f*) inulin. *B*, mean apparent sucrose permeability (±S.E. of mean, $n = 24$) compared with control data obtained at normal osmolality ($n = 4$). *C*, mean volume flow rates (±S.E. of mean, $n = 24$) compared with control data as in *B*. The data are all based on 1 hr absorbate samples.

DISCUSSION

In the past, non-electrolyte permeability studies of the rabbit gall-bladder epithelium (Wright & Diamond, 1969; Smulders & Wright, 1971; van Os *et al.* 1974) have been carried out under experimental conditions where fluid transport rates can be presumed to be very low. Evidence has accumulated for the existence of three

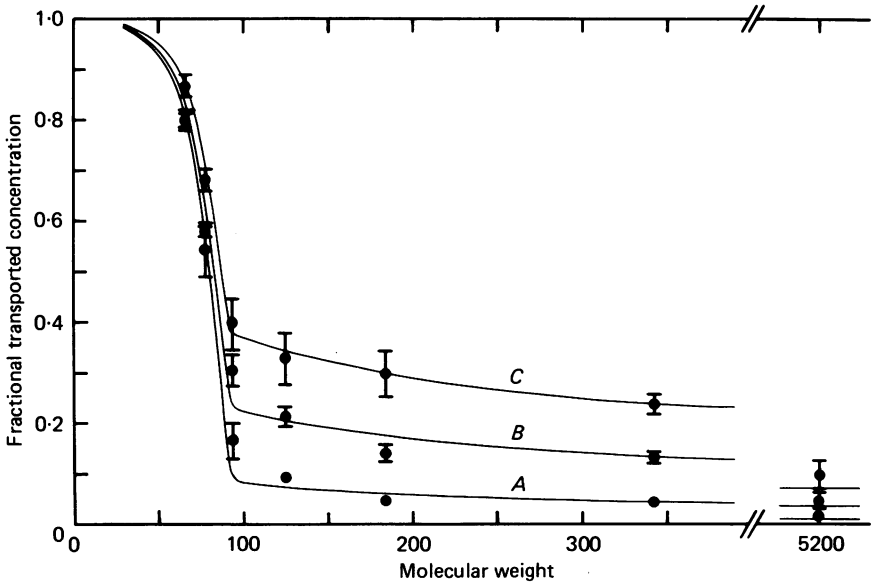

Fig. 10. Non-electrolyte selectivity patterns immediately before (*A*) and over two 1 hr periods after the reduction of the mucosal osmolality to 110 m-osmole kg^{-1} (*B* and *C*). The three curves were generated by the slit model using the junctional parameters established in Fig. 7*A*. They differ only in the values used for the sucrose permeabilities and volume flow rates which were taken from the experimental data. *A*, normal osmolality: $P_{su}' = 1{\cdot}0 \times 10^{-6}$ cm sec^{-1}, $J_v = 77$ $\mu l \,.\, cm^{-2}$ hr^{-1}. *B*, mean values from the period 1–2 hr after the reduction of the mucosal osmolality: $P_{su}' = 3{\cdot}2 \times 10^{-6}$ cm sec^{-1}, $J_v = 73$ $\mu l \,.\, cm^{-2}$ hr^{-1}. *C*, mean values from the period 3–4 hr after the reduction of the mucosal osmolality: $P_{su}' = 4{\cdot}7 \times 10^{-6}$ cm sec^{-1}, $J_v = 54$ $\mu l \,.\, cm^{-2}$ hr^{-1}.

principal routes of passive non-electrolyte permeation: (i) a transcellular permeability to lipid-soluble non-electrolytes; (ii) an anomalous additional permeability to small polar non-electrolytes; and (iii) a rather variable but generally low paracellular 'shunt' permeability available to molecules at least as large as inulin. The second of these three routes was attributed initially to a polar pathway through the epithelial cell membranes (Wright & Diamond, 1969). More recently though, Moreno (1975*b*) has demonstrated that 2,4,6-triaminopyrimidinium (TAP), which blocks the paracellular cation channels, also reduces the permeability to small polar non-electrolytes, so there may in addition, or alternatively, be a substantial paracellular permeability to these smaller molecules.

Naturally any of these three or four non-electrolyte permeation routes will be available to water molecules, so if a full understanding of epithelial water transport is to be achieved, it is important that the contribution of each route to both passive (osmotically induced and pressure-induced) water flows, and, more importantly, to 'active' isotonic water transport be determined. What would appear the simplest way of approaching this question would be to look for evidence of solvent drag in the fluxes of non-electrolytes known to take particular routes across the epithelium. For example, the observation of almost unrestricted sucrose tracer flow during fluid transport in *Necturus* gall-bladder (Hill & Hill, 1978*a*) indicates that in that tissue there is a substantial flow of water through relatively wide channels in the

paracellular pathway. Previous work, however, suggests that the situation is quite different in the rabbit gall-bladder. In that epithelium, although a significant sucrose permeability is evident in the absence of fluid transport ($1{\cdot}8 \times 10^{-6}$ cm sec^{-1}, Moreno, 1975*b*), relatively little sucrose appears in the absorbate during fluid transport (Diamond, 1964*b*).

Non-electrolyte permeation at normal osmolality

The results of the present study suggest that the small sucrose fluxes observed in the rabbit epithelium during fluid transport are actually no greater than would be expected from passive diffusion through a 'shunt' or 'leakage' permeability of $1{\cdot}1 \times 10^{-6}$ cm sec^{-1}. The absence of any enhancement of sucrose permeation during fluid transport would seem to indicate that very little of the water flow across the rabbit epithelium follows the paracellular shunt pathway. On the other hand, the smaller non-electrolyte molecules ethanediol and thiourea appear to penetrate the epithelium quite freely. It is possible, therefore, that the apparent fundamental difference between the *Necturus* and rabbit epithelia is simply the result of a difference between the effective diameters of their restricted junctional channels. Before this explanation can be accepted with confidence though, two questions have to be answered: (i) might the appearance of ethanediol and thiourea tracers in the absorbate be a result of transcellular non-electrolyte permeation? and (ii) if we can assume that these small non-electrolytes are largely confined to the paracellular pathway, do their fluxes necessarily indicate significant paracellular water flow?

If the slow exponential component observed in the efflux of the smaller tracer non-electrolytes from preloaded gall-bladder pieces truly reflects efflux from the cellular compartment, it is clear that the transcellular permeabilities to ethanediol and thiourea are much too small to account for the transepithelial fluxes seen during fluid transport. The reflexion coefficient measurements of Wright & Diamond (1969) support this conclusion. In addition, it has been observed that application of 10^{-3} M-ouabain to both sides of a bilateral rabbit gall-bladder preparation reduces its apparent thiourea permeability by at least 95% (Steward, 1979). Since treatment with ouabain is believed to bring about the almost total occlusion of the interspaces as a result of epithelial cell swelling (Tormey & Diamond, 1967), this result too is consistent with the idea that the paracellular pathway is responsible for the bulk of the transepithelial thiourea permeability.

If it can be accepted that ethanediol and thiourea cross the gall-bladder epithelium mainly via restricted channels through the intercellular junctions, it remains to be established whether the observed large fluxes through these channels are the result of a large diffusive permeability which allows the non-electrolytes to enter a standing-gradient flow stream in the interspace by diffusion, or whether they indicate solvent drag associated with a flow of water through the junctional channels. Superficially, the hydrodynamic model that has been examined in the present investigation would appear to support the latter alternative. In order to generate the high f_n values characteristic of ethanediol and thiourea, and yet exclude molecules larger than glycerol, the model requires a paracellular water flow certainly well in excess of one half of the total transepithelial flow. Further consideration, however, reveals that this is not because the ethanediol and thiourea fluxes have to be

interpreted in terms of solvent drag through the junctional channels. It is actually because in the absence of substantial paracellular water flow, a standing-gradient flow pattern would generate a poorly stirred region at the junctional end of the interspace which would act as a major barrier to non-electrolyte entry by diffusion (Steward, 1981).

Even though it seems likely that the bulk of the transepithelial water flow passes through the restricted junctional channels, solvent drag *per se* probably does not contribute as much as diffusion to the passage of ethanediol and thiourea through these channels at normal volume flow rates. This conclusion derives from an estimate of the expected diffusive and convective (solvent drag) components of the non-electrolyte fluxes, which may be obtained by inserting the channel dimensions and drag factors indicated by the model studies into an approximate expression for solute flow (see Appendix, eqn. (A 13)):

$$J_n = \frac{S_D}{K_1}\frac{2rs}{n}D_n(C_n(M)-C_n(0))+\frac{S_F K_2}{K_1}pJ_v\frac{C_n(M)+C_n(0)}{2}. \quad (15)$$

It seems that even when all the transepithelial water flow is made to follow the paracellular route, i.e. $p = 1$, the diffusive component has to contribute the majority of the ethanediol flux (81 % in this instance) in order to achieve the observed emergent absorbate concentration. This is because junctional channels narrow enough to exclude molecules larger than glycerol will impede convective ethanediol flow to the extent that the filtration reflexion coefficient, $1-S_F K_2/K_1$ (see Appendix), is of the order of 0·84.

Non-electrolyte permeation at reduced osmolality

In view of previous observations (Diamond, 1964*b*), it was to be expected that a reduction of the mucosal Ringer solution osmolality to approximately 110 m-osmole kg^{-1} might bring about an increase in the apparent sucrose permeability of the unilateral preparation. The increase that was observed in fact occurred steadily over a period of at least 4 hr (Fig. 9*B*), and it would appear from the changes in the non-electrolyte selectivity pattern as a whole (Fig. 10) to have been the result of a progressive increase in the magnitude of the unrestricted shunt component of the paracellular permeability rather than a change in the selectivity of the restricted junctional channels. It is impossible to tell from the experimental data, however, whether the increased shunt permeability was due to disruption of epithelial integrity on account of cell death for example, or whether it was the result of the 'opening' of some regions of the junctional network.

Very recently, Whittembury *et al.* (1980) have published the results of a study of epithelial non-electrolyte permeation in the unilateral guinea-pig gall-bladder preparation. Perhaps surprisingly, the guinea-pig epithelium, unlike the rabbit epithelium, appears to allow quite substantial mucosa-to-serosa fluxes of sucrose, inulin and dextran tracers during fluid transport. At normal osmolality the fractional transported concentrations reported were 0·40, 0·33 and 0·10 respectively. Because of the low volume flow rates however (approximately 9 μl. cm^{-2} hr^{-1}) these data correspond to apparent permeabilities of only 1·7, 1·2 and $0{\cdot}3 \times 10^{-6}$ cm sec^{-1}, which are quite comparable with the permeabilities attributed to the unrestricted shunt

pathway in the rabbit. On account of the apparent J_v dependence of the non-electrolyte fluxes, though, Whittembury *et al.* interpret their data in terms of solvent drag through paracellular channels of 20–40 Å radius. This interpretation depends rather heavily on fluxes determined at very low osmolality (20 m-osmole kg^{-1}) and it is possible that an elevated shunt permeability, such as is observed in the rabbit gall-bladder under less severe conditions, is a complicating factor which needs to be eliminated. If, on the other hand, the analysis of Whittembury *et al.* proves to be correct, their results suggest that the guinea-pig gall-bladder epithelium is an unusually leaky mammalian epithelium, and this observation, like that of Hill & Hill (1978*a*) in *Necturus*, will inevitably impose considerable constraints on the possible driving forces envisaged for junctional water flow (Hill, 1980).

The nature of the junctional channels

In view of the many simplifying assumptions underlying the junctional models considered in this paper, the geometry and precise dimensions suggested by simulations of non-electrolyte flow cannot be regarded as more than a very rough indication of the possible channel structure. The radius or half-width of the channels responsible for the restricted permeability, however, must be close to 3 Å to allow ethanediol and thiourea, but not erythritol or mannitol, to penetrate the junctions by this route. It is interesting to note, therefore, that the junctional cation channels characterized in this epithelium by Moreno & Diamond (1975) are of approximately the same size ($r = 4{\cdot}4$ Å). It is also perhaps significant, in view of the difference between the rabbit and *Necturus* non-electrolyte selectivities, that the cation channels of another amphibian, *Rana catesbeiana*, are apparently considerably larger than those of the rabbit ($r = 8{\cdot}1$ Å, Moreno & Diamond, 1975). These comparisons naturally raise the possibility that the junctional cation channels are responsible for the large restricted non-electrolyte permeability that was observed in this study. Some support for this hypothesis comes from the observation that TAP, which significantly reduces the permeability of the cation channels, also reduces the epithelial permeability to urea and glycerol (Moreno, 1975*a*, *b*). If the hypothesis is correct, the present results suggest that the junctional cation channels may carry the bulk of the water flow crossing the epithelium during isotonic fluid transport.

APPENDIX

Non-electrolyte flow in the junctional channels

Unrestricted non-electrolyte flow by convection and diffusion in a channel of cross-sectional area A containing a moving fluid, is adequately described at any distance x along the channel by

$$\frac{j_n(x)}{A} = v(x)\,C_n(x) - D_n \frac{dC_n}{dx}(x), \tag{A 1}$$

where $v(x)$ and $C_n(x)$ are the fluid velocity and non-electrolyte concentration, and D_n the free-solution diffusion coefficient. If, however, as in the restricted junctional channels, the solute radius a_n exceeds even a very small fraction of the effective channel radius r, eqn. (A 1) has to be modified substantially (Renkin & Curry, 1979)

to take into account: (i) steric restrictions on the position of the non-electrolyte molecules in the channel and (ii) hydrodynamic drag effects due to the proximity of the channel wall:

$$\frac{j_n(x)}{A} = \frac{S_F K_2}{K_1} v(x) C_n(x) - \frac{S_D}{K_1} D_n \frac{dC_n}{dx}(x). \quad (A\,2)$$

Here, S_F and S_D are steric restriction factors for convective and diffusive flow which depend on: (i) the ratio λ of the solute radius and the channel radius (or half-width), (ii) the geometry of the channel, and (iii) the nature of the fluid flow within the channel. In a cylindrical pore through which the fluid flow is laminar, the fractions of the channel cross section effectively available for convection and diffusion of the solute are

$$S_F = 2(1-\lambda)^2 - (1-\lambda)^4, \quad (A\,3)$$

$$S_D = (1-\lambda)^2 \quad (A\,4)$$

and in a parallel-sided slit the equivalent expressions are

$$S_F = \tfrac{2}{3}(1-\lambda) - \tfrac{1}{2}(1-\lambda)^3, \quad (A\,5)$$

$$S_D = 1-\lambda. \quad (A\,6)$$

The hydrodynamic drag factors K_2/K_1 and $1/K_1$ applicable to the cylindrical pore may be approximated (Haberman & Sayre, 1958) by:

$$\frac{K_2}{K_1} = \frac{1-\frac{2}{3}\lambda^2 - 0{\cdot}20217\lambda^5}{1-0{\cdot}75857\lambda^5}, \quad (A\,7)$$

$$\frac{1}{K_1} = \frac{1-2{\cdot}105\lambda + 2{\cdot}0865\lambda^3 - 1{\cdot}7068\lambda^5 + 0{\cdot}72603\lambda^6}{1-0{\cdot}75857\lambda^5} \quad (A\,8)$$

and those for the parallel-sided slit (Happel & Brenner, 1965) by

$$\frac{K_2}{K_1} = 1-\tfrac{1}{3}\lambda^2, \quad (A\,9)$$

$$\frac{1}{K_1} = 1-1{\cdot}004\lambda + 0{\cdot}418\lambda^3 - 0{\cdot}210\lambda^4 - 0{\cdot}169\lambda^5. \quad (A\,10)$$

The combined correction factors for restricted convective and diffusive non-electrolyte flow, $S_F K_2/K_1$ and S_D/K_1, are plotted as functions of λ for both pores and slits in Fig. 11.

The expected steady-state non-electrolyte flux J_n through the restricted junctional channels of 1 cm^2 of epithelium may be estimated by integrating eqn. (A 2) over the length and total cross-sectional area of the channels occupying that area of epithelium. This yields an expression for J_n in terms of the non-electrolyte concentrations at either end of the channels, $C_n(M)$ and $C_n(0)$, and the junctional volume-flow pJ_v per cm^2 of epithelium (Fig. 6). In the case of a population of N cylindrical pores of radius r, and depth n, integration of eqn. (A 2) gives

$$J_n(\text{pore}) = \frac{S_F K_2}{K_1} pJ_v \frac{C_n(M)\exp\left(\frac{S_F K_2}{S_D}\frac{pJ_v}{N\pi r^2}\frac{n}{D_n}\right) - C_n(0)}{\exp\left(\frac{S_F K_2}{S_D}\frac{pJ_v}{N\pi r^2}\frac{n}{D_n}\right) - 1}. \quad (A\,11)$$

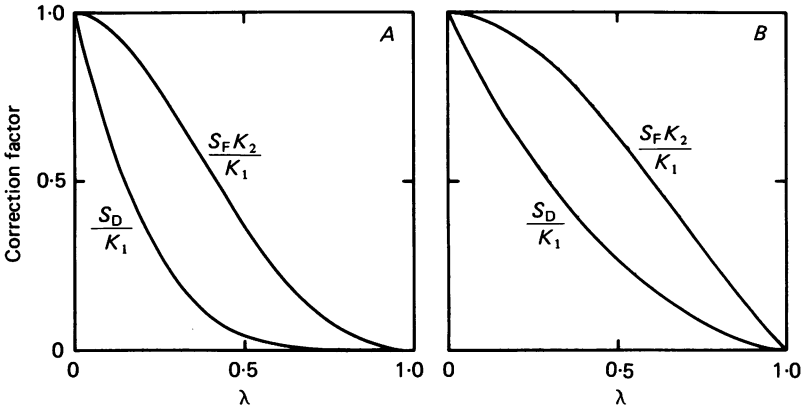

Fig. 11. Combined steric exclusion and hydrodynamic drag factors restricting the diffusive (S_D/K_1) and convective ($S_F K_2/K_1$) flow of a spherical solute in a narrow channel, plotted as a function of the solute:channel radius ratio A, cylindrical pore. B, parallel-sided slit.

If the restricted channels form a network of parallel-sided slits of half-width r, depth n and linear extent s in the plane of the epithelium, integration gives

$$J_n(\text{slit}) = \frac{S_F K_2}{K_1} pJ_v \frac{C_n(M)\exp\left(\frac{S_F K_2}{S_D}\frac{pJ_v}{2rs}\frac{n}{D_n}\right) - C_n(0)}{\exp\left(\frac{S_F K_2}{S_D}\frac{pJ_v}{2rs}\frac{n}{D_n}\right) - 1}. \quad \text{(A 12)}$$

It will be noted that in eqns. (A 11) and (A 12) the junctional parameters N and s occur in association with the junction depth n. This means that for the purposes of analysis, it is possible to treat N/n and s/n as single parameters. It may also be noted that under conditions where the arguments of the exponential terms in eqns. (A 11) and (A 12) are small, and where $C_n(M) \approx C_n(0)$, the expressions are approximated (Bean, 1972) by the solute flux equation of Kedem & Katchalsky (1958)

$$J_n = \omega_n RT\Delta C_n + (1-\sigma)pJ_v\bar{C}_n \quad \text{(A 13)}$$

in which:
$$\omega_n RT = \frac{S_D}{K_1}\frac{N\pi r^2}{n}D_n \text{ or } \frac{S_D}{K_1}\frac{2rs}{n}D_n$$

and
$$1-\sigma = \frac{S_F K_2}{K_1}.$$

The mean apparent permeability to sucrose P_{su}' (Table 1) may be used to estimate the additional flux of each non-electrolyte J_n(shunt) that passes through the non-selective shunt permeability presumed to exist in parallel with the restricted junctional channels described above:

$$J_n(\text{shunt}) = P_{su}'\frac{D_n}{D_{su}}(C_n(M) - C_n(0)). \quad \text{(A 14)}$$

Non-electrolyte flow in the interspace

If the interspace is treated as a uniform parallel-sided space of constant half-width R, length L and linear extent l (per cm^2) in the plane of the epithelium, and if

non-electrolyte flow by convection and diffusion is largely unrestricted, eqn. (A 1) becomes

$$J_n = 2Rlv(x)\,C_n(x) - 2RlD_n\frac{dC_n}{dx}(x) \qquad (A\,15)$$

where x refers to the distance from the tight-junction end of the interspace (Fig. 6). The fluid velocity profile along the interspace $v(x)$ will depend upon the distribution of flow between the paracellular and transcellular pathways (pJ_v and $(1-p)J_v$), and on the distribution of the latter over the lateral membranes of the epithelial cells. If the transcellular component is to satisfy the differential equations for standing-gradient osmotic flow with uniformly distributed salt transport (Diamond & Bossert, 1967) and yield a fluid isotonic with the mucosal Ringer solution to within 1%, it can be shown (Hill & Hill, 1978*a*; Hill, A. E., personal communication) that the over-all velocity profile, including the paracellular component, is well approximated by

$$2Rlv(x) = pJ_v + (1-p)J_v\left[-1{\cdot}68\left(\frac{x}{L}\right)^4 + 4{\cdot}58\left(\frac{x}{L}\right)^3 - 5{\cdot}2\left(\frac{x}{L}\right)^2 + 3{\cdot}3\left(\frac{x}{L}\right)\right]. \qquad (A\,16)$$

Values for R and l have been taken as 0·465 μm (Blom & Helander, 1977) and 4000 cm cm^{-2} (Steward, 1979).

In the steady state, the non-electrolyte flux through the junction has to equal that along the interspace. The particular value of J_n which satisfies this condition may be determined by finding iteratively the value of $C_n(0)$ which on insertion into eqns. (A 11) or (A 12) and (A 14), and when used as a boundary condition for the solution of the interspace flow eqn. (A 15) yields identical fluxes through the two parts of the paracellular pathway. This procedure may be carried out by computer and the expected fractional transported concentrations of the non-electrolytes obtained by setting $C_n(M)$ to unity, whence

$$f_n = J_n/J_v. \qquad (A\,17)$$

I am very grateful to Drs A. E. and B. S. Hill for their invaluable advice and guidance, to Professor R. D. Keynes for his support and encouragement, and to Professors J. A. Young and R. M. Case for helpful suggestions during the preparation of the manuscript. The experimental work was carried out during tenure of a Medical Research Council research studentship.

REFERENCES

Bean, C. P. (1972). The physics of porous membranes – neutral pores. In *Membranes*, vol. 1, ed. Eisenman, G. New York: Dekker.

Berry, C. A. & Boulpaep, E. L. (1975). Nonelectrolyte permeability of the paracellular pathway in *Necturus* proximal tubule. *Am. J. Physiol.* **228**, 581–595.

Blom, H. & Helander, H. F. (1977). Quantitative electron microscopical study of *in vitro* incubated rabbit gall bladder epithelium. *J. membrane Biol.* **37**, 45–61.

Diamond, J. M. (1964*a*). Transport of salt and water in rabbit and guinea pig gall bladder. *J. gen. Physiol.* **48**, 1–14.

Diamond, J. M. (1964*b*). The mechanism of isotonic water transport. *J. gen. Physiol.* **48**, 15–42.

Diamond, J. M. (1979). Osmotic water flow in leaky epithelia. *J. membrane Biol.* **51**, 195–216.

Diamond, J. M. & Bossert, W. H. (1967). Standing gradient osmotic flow: a mechanism for coupling of salt and water transport in epithelia. *J. gen. Physiol.* **50**, 2061–2083.

Haberman, W. L. & Sayre, R. M. (1958). Motion of rigid and fluid spheres in stationary and moving liquids inside cylindrical tubes. In *David Taylor Model Basin Hydromechanics Lab. R. & D, report no. 1143*. U.S. Dept. of the Navy.

HAPPEL, J. & BRENNER, H. (1965). *Low Reynolds Number Hydrodynamics*. Englewood Cliffs, NJ: Prentice-Hall.

HILL, A. E. (1980). Salt-water coupling in leaky epithelia. *J. membrane Biol.* **56**, 177–182.

HILL, A. E. & HILL, B. S. (1978*a*). Sucrose fluxes and junctional water flow across *Necturus* gall bladder epithelium. *Proc. R. Soc.* B. **200**, 163–174.

HILL, B. S. & HILL, A. E. (1978*b*). Fluid transfer by *Necturus* gall bladder epithelium as a function of osmolality. *Proc. R. Soc.* B. **200**, 151–162.

HUNTER, M., CASE, R. M., STEWARD, M. C. & YOUNG, J. A. (1981). The permeability and reflection coefficients of the perfused rabbit mandibular salivary gland to non-electrolytes. In *Electrolyte and Water Transport across Gastrointestinal Epithelia*, ed. CASE, R. M., GARNER, A., TURNBERG, L. & YOUNG, J. A. New York: Raven.

KEDEM, O. & KATCHALSKY, A. (1958). Thermodynamic analysis of the permeability of biological membranes to nonelectrolytes. *Biochim. biophys. Acta* **27**, 229–246.

LONGSWORTH, L. G. (1953). Diffusion measurements, at 25 °C, of aqueous solutions of amino acids, peptides and sugars. *J. Am. chem. Soc.* **75**, 5705–5709.

MORENO, J. H. (1975*a*). The blockage of gall bladder tight junction cation selective channels by 2,4,6-triaminopyrimidinium. *J. gen. Physiol.* **66**, 97–115.

MORENO, J. H. (1975*b*). Routes of nonelectrolyte permeability in gallbladder. Effects of 2,4,6-triaminopyrimidinium (TAP). *J. gen. Physiol.* **66**, 117–128.

MORENO, J. H. & DIAMOND, J. M. (1975). Nitrogenous cations as probes of permeation channels. *J. membrane Biol.* **21**, 197–259.

OS, C. H. VAN, DE JONG, M. D. & SLEGERS, J. F. G. (1974). Dimensions of polar pathways through rabbit gall bladder epithelium. The effect of phloretin on nonelectrolyte permeability. *J. membrane Biol.* **15**, 363–382.

PHELPS, C. F. (1965). The physical properties of inulin solutions. *Biochem. J.* **95**, 41–47.

RENKIN, E. M. & CURRY, F. E. (1979). Transport of water and solutes across capillary endothelium. In *Membrane Transport in Biology*, vol. IVA, ed. GIEBISCH, G., TOSTESON, D. C. & USSING, H. H. Berlin-Heidelberg-New York: Springer-Verlag.

SCHULTZ, S. G. & SOLOMON, A. K. (1961). Determination of the effective hydrodynamic radii of small molecules by viscometry. *J. gen. Physiol.* **44**, 1189–1199.

SMULDERS, A. P. & WRIGHT, E. M. (1971). The magnitude of nonelectrolyte selectivity in the gallbladder epithelium. *J. membrane Biol.* **5**, 297–318.

STEIN, W. D. (1967). *The Movement of Molecules across Cell Membranes*. New York–London: Academic.

STEWARD, M. C. (1979). The role of the paracellular pathway in epithelial fluid transport. Ph.D. Thesis. University of Cambridge, England.

STEWARD, M. C. (1981). Paracellular transport in the gall bladder. In *Electrolyte and Water Transport across Gastrointestinal Epithelia*, ed. CASE, R. M., GARNER, A., TURNBERG, L. & YOUNG, J. A. New York: Raven.

TORMEY, J. McD. & DIAMOND, J. M. (1967). The ultrastructural route of fluid transport in rabbit gall bladder. *J. gen. Physiol.* **50**, 2031–2060.

WHITTEMBURY, G., MARTINEZ, C. V. DE, LINARES, H. & PAZ-ALIAGA, A. (1980). Solvent drag of large solutes indicates paracellular water flow in leaky epithelia. *Proc. R. Soc.* B. **211**, 63–81.

WRIGHT, E. M. & DIAMOND, J. M. (1969). Patterns of non-electrolyte permeability. *Proc. R. Soc.* B. **172**, 227–271.